



Can state-of-the-art infrared satellite sounders and reanalyses detect moisture inversions in the Arctic?

Giovanni Chellini¹ and Kerstin Ebell¹

¹Institute for Geophysics and Meteorology, University of Cologne, Cologne, Germany

Correspondence: Giovanni Chellini (g.chellini@uni-koeln.de)

Abstract. Moisture inversions, i.e. layers in the troposphere where specific humidity increases with height, are extremely frequent in the Arctic. They are strongly intertwined with cloud processes, as well as the energy budget, by affecting the downward longwave radiation. In this study, the capability of two benchmark satellite sounders, the Infrared Atmospheric Sounding Interferometer (IASI) and the Atmospheric Infrared Sounder (AIRS), to detect moisture inversions is systematically assessed based on radiosonde data from the Arctic site Ny-Ålesund. In particular for IASI, such an analysis has not been done before. The frequency of occurrence of moisture inversions at Ny-Ålesund based on radiosoundings is above 95 % in all seasons, with multiple inversions in the same profile occurring most of the time (in 82 % of the profiles). We first performed a sensitivity analysis which revealed that the chosen vertical grid of the specific humidity profiles has a distinct impact on the inversion frequency: in general, the lower the grid resolution, the lower also the detected inversion frequency. However, even when reducing the vertical resolution of the radiosonde profiles used in the comparison to match that of the IASI and AIRS retrievals, a large underestimation in both inversion frequency and inversion strength can be found in the satellite products. While observed inversion frequency in any 100-hPa-deep layer between 1000 and 400 hPa is typically between 10 and 20 % (50 and 80 %) in the regridded (original) radiosonde data, inversion frequency in satellite data is in most cases below 10 %. A better agreement has been found for IASI below the 900-hPa level and in particular for winter, while AIRS does not detect any inversions below the 700-hPa level in this season. In addition to satellite data, reanalysis data also have the potential to provide an Arctic-wide view on moisture inversion characteristics. Here, we thus also assessed the capability of the latest reanalysis developed by ECMWF, ERA5, to detect moisture inversions at Ny-Ålesund, by performing a similar comparison with radiosoundings. We found that ERA5 represents Arctic moisture inversion characteristics very well, if the radiosonde profile resolution is reduced to that of the reanalysis.

20 1 Introduction

In the past decades the Arctic region has undergone drastic changes, most notably the dramatic decline in sea ice extent, which decreased by one third within the last 50 years (Stroeve et al., 2012; Jeffries et al., 2013). Concurrently, the Arctic region has been subject to a greater warming compared to lower latitudes: this phenomenon has been termed Arctic amplification and is evident in annual surface air temperature trends for the past 60 years (Serreze and Barry, 2011). Since the mid-1990s the Arctic has in fact warmed at a rate that is double the global mean temperature increase (Serreze and Barry, 2014). At the same time,



Arctic amplification is a feature found in most major climate model simulations, when accounting for increasing atmospheric greenhouse gas concentrations (Serreze and Barry, 2011; Langen et al., 2012).

Despite the magnitude of these changes, our understanding of the processes causing Arctic amplification is still far from complete. In particular, clouds and atmospheric water vapor strongly affect the energy budget through radiative fluxes and are thus thought to play a substantial role in Arctic amplification (Serreze and Barry, 2011; Vihma et al., 2016). However, due to the unique conditions found at high latitudes, many processes involving clouds and atmospheric moisture show characteristics that are Arctic-specific, most notably the wide occurrence of mixed-phase clouds (e.g. Morrison et al., 2012) and of moisture inversion layers (e.g. Nygård et al., 2014). Specific humidity, in fact, typically decreases with height, but moisture inversions, i.e. layers where specific humidity increases with height, have been found to occur frequently at high latitudes and simultaneously at several height levels (Nygård et al., 2013, 2014). Their wide occurrence has major implications for cloud formation, as they have been found to provide a moisture source for cloud layers allowing for persistent cloud cover (Morrison et al., 2012), as well as clear-sky radiative transfer as they increase downward longwave radiation (Devasthale et al., 2011). Despite their role in the energy budget and in cloud processes, in the past decade just a handful of studies addressed their climatology and formation mechanisms, i.e. Devasthale et al. (2011), Nygård et al. (2014), Brunke et al. (2015), Maturilli and Kayser (2017) and Naakka et al. (2018).

Nygård et al. (2014) estimated their frequency of occurrence to range from 90 % to 100 % in winter, and from 70 % to 90 % in summer, using radiosonde data taken from several launch sites across the Arctic region. Nygård et al. (2014) found that nearly 80 % of them are not surface-based, and that only a fraction of moisture inversions is linked to temperature inversions, between 30 % and 80 % depending on the site.

Most authors that studied moisture inversions characterized them via inversion strength, in addition to their frequency of occurrence (Devasthale et al., 2011; Nygård et al., 2014; Naakka et al., 2018; Chang et al., 2021). Nygård et al. (2014) defined the moisture inversion strength as the difference between specific humidity at inversion top and inversion base. With this definition applied to radiosonde data, the authors found that median values of inversion strength range from 0.1 to 0.3 g kg⁻¹ in winter to 0.3 to 0.6 g kg⁻¹ in summer depending on the location (Nygård et al., 2014). Unlike the other studies, Maturilli and Kayser (2017) quantified the intensity of moisture inversions by estimating the contribution of the inversion layer to the Integrated Water Vapor (IWV) based on radiosondes launched at Ny-Ålesund. They found that moisture inversions on average contribute to approximately 10 % of the total IWV.

Naakka et al. (2018) obtained moisture inversion statistics across the Arctic from the ERA-Interim and JRA-55 reanalyses. They found a wide geographical variability of moisture inversion characteristics. On the one hand, in winter, inversion frequency is close to 100 % across the frozen Arctic Ocean and the continents, while it is drastically lower over the North Atlantic and North Pacific Oceans. On the other hand, in summer, moisture inversion frequency falls below 50 % over the continents, and ranges between 70 to 90 % across the Arctic Ocean, where the maximum in mean strength is observed. A clear seasonal cycle is thus present below the 800-hPa level. Above the 800-hPa level, Naakka et al. (2018) found a uniform frequency of occurrence of approximately 40 % in every 100-hPa-thick layer, up to 400 hPa.



60 This seasonal and geographical variability can be attributed to the distribution of the two processes leading to the formation
of moisture inversions: moisture advection and condensation in an atmospheric layer. In winter, strong surface radiative cooling
leads to surface-based temperature inversions, that induce saturation and condensation in the lowest layers of the troposphere,
thus leading to the formation of a low-level moisture inversion. In summer, low-level moisture inversions are often originated
by advection of warm moist air masses over the cold ocean surface resulting in cooling and saturation in the lowest layers
65 (Naakka et al., 2018). In non-saturated conditions they are caused by moisture advection, especially by large-scale transport
and atmospheric rivers (Brunke et al., 2015). Since temperature inversions mostly occur near the surface, moisture inversions
above the 800-hPa level originate, for the most part, from moisture advection. Below this level, moisture inversions can arise
from both advection and condensation, as they might be linked to the surface energy budget (Naakka et al., 2018).

As already mentioned, Arctic moisture inversions have received very little attention in literature. Radiosonde launches are
70 very sparse across the Arctic, leaving large unsampled areas over the Arctic ocean and inland regions of the continents (Dev-
asthale et al., 2011). This means that Arctic-wide analyses of moisture inversions need to rely on reanalyses and satellite
remote sensing. However, reanalyses have been found to show large uncertainties in representing moisture inversions. Brunke
et al. (2015) performed a global study of moisture inversions using five reanalyses (NCEP-2, ERA-40, MERRA, CFSR, ERA-
Interim), while Naakka et al. (2018) obtained moisture inversion statistics across the Arctic from ERA-Interim and JRA-55.
75 Both studies observed that in radiosoundings, Arctic moisture inversions are in general stronger and more frequent than in the
reanalyses. Furthermore, they found substantial disagreements between results from different reanalyses.

Nowadays satellite-based infrared sounders are routinely used to retrieve temperature and humidity profiles for numerical
weather prediction and climate studies (e.g. Menzel et al., 2018). However, they only provide a limited number of degrees of
freedom for signal, i.e. independent pieces of information, in the retrieved profiles. Consequently, the retrieved temperature and
80 humidity profiles appear smoother than e.g. radiosoundings, and complex features in the profiles, such as inversions, might not
be captured (e.g. Löhnert et al., 2009). This effect can be clearly seen in Fig. 1, where examples of specific humidity profiles
from IASI and AIRS together with the corresponding radiosonde profile at Ny-Ålesund are shown (for the sampling of the
satellite data see Sect. 3.3). This also implies that capturing moisture inversions is quite challenging from a satellite-based
perspective. Furthermore, even if an inversion is captured it might have its characteristics, such as height, depth, and strength
85 (i.e. difference in specific humidity between inversion top and bottom) misrepresented.

There has been just one attempt to study Arctic moisture inversions employing such instruments by Devasthale et al. (2011)
who analyzed retrievals from the Atmospheric Infrared Sounder (AIRS). However, in a subsequent study by Nygård et al.
(2014) who analyzed moisture inversion statistics from radiosoundings and compared their results to the results of Devasthale
et al. (2011), it was shown that inversion frequency is substantially underestimated when derived from the AIRS humidity
90 profiles.

Retrievals from the Infrared Atmospheric Sounding Interferometer (IASI) have never been used to study Arctic moisture
inversions. The instrument performance in literature suggests that IASI could provide an alternative means of studying these
phenomena (Aires, 2011; Ebell et al., 2013). Furthermore, IASI measures across a broader spectral range compared to AIRS.
Thus, one main objective of this study is assessing the capability of IASI to detect Arctic moisture inversions. The analysis will



95 be performed based on both IASI and AIRS products. Here, we focus on the year 2017. As reference data, humidity profiles from radiosondes launched at the AWIPEV research station at Ny-Ålesund, Svalbard, will be used. At AWIPEV, radiosondes are launched operationally at least once per day.

As a further objective, the performance in representing moisture inversions of the ERA5 reanalysis (Hersbach et al., 2019) is also assessed using a similar methodology. ERA5 is the most recent reanalysis produced by ECMWF and, to our knowledge, 100 its performance in representing Arctic moisture inversions has only been assessed by Chang et al. (2021). ERA5 performance is expected to improve upon that of its predecessor, ERA-Interim (Berrisford et al., 2011), which showed shortcomings in its representation of Arctic moisture inversions (Naakka et al., 2018). While observing improvements in ERA5, when comparing it to ERA-Interim, Chang et al. (2021) found several limitations in the reanalysis ability to capture the characteristics of moisture inversions. The authors in fact compared inversion statistics from ERA5 and ERA-Interim with similar statistics from 105 radiosondes launched during three shipborne campaigns in the Arctic ocean. They reported significant discrepancies in the occurrence of profiles containing moisture inversions. They in particular highlighted an underestimation of occurrence (up to 50 percentage points) and strength of surface-based moisture inversions.

After presenting the data sets used (Sect. 2) and methods applied (Sect. 3), we will first show results of a long-term moisture inversion climatology above Ny-Ålesund using 11 years (1 January 2007 - 31 December 2017) of radiosonde data (section 4.1). 110 These statistics are then compared to identical statistics performed on 2017 only to check for representativity of this year, which is used in the analysis of the satellite and reanalysis data. In a next step, we will also assess the impact of the chosen vertical grid on the ability to capture moisture inversions (Sect. 4.2). The motivation for this exercise is that differences in diagnosed moisture inversion characteristics from different data sets are likely also due to the different vertical grids used (Chang et al., 2021). Also, in order to allow for a fairer comparison of the vertically highly resolved radiosonde data to coarser 115 resolved humidity profiles of AIRS, IASI and ERA-5, the vertical resolution of the radiosonde profiles needs to be reduced correspondingly. In Sect. 4.3, the ability of IASI and AIRS products to resolve moisture inversions is assessed. Section 4.4 focuses on the performance of ERA5 in representing moisture inversions followed by conclusions and an outlook in Sect. 5.

2 Data sets

2.1 Radiosondes

120 Radiosondes are widely used to measure vertical profiles of several atmospheric variables at a high number of sites around the world. They provide a highly vertically resolved and reliable profile, performing measurements every 2 to 10 seconds during their ascent, typically from the ground level to the mid-stratosphere. Despite certain known instrumental problems, such as a slower response in cold air, contamination by clouds, and a dry radiation bias, they still provide the most accurate and reliable means of measuring vertical humidity profiles.

125 We use profiles from radiosondes launched from the AWIPEV station, located at the high-Arctic coastal site of Ny-Ålesund, Svalbard, between 1st January 2007 and 31st December 2017. At said station radiosondes are launched daily at 12 UTC with additional radiosondes being launched during measurement campaigns.

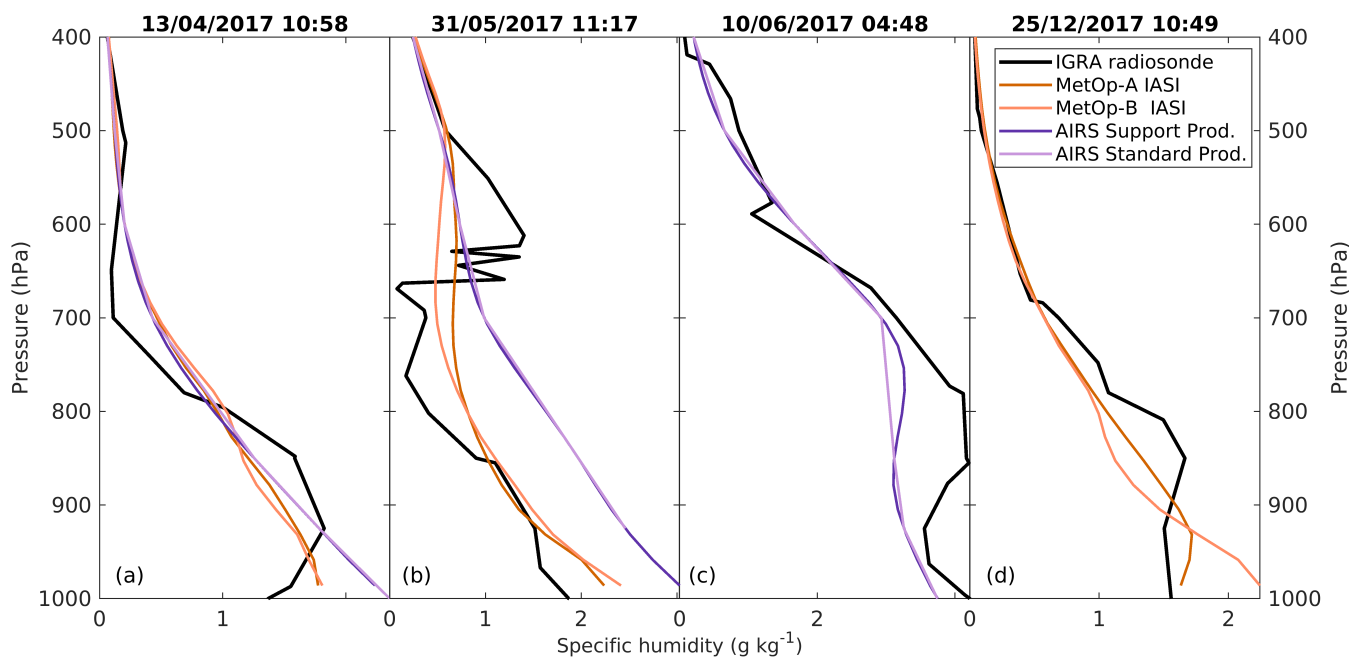


Figure 1. Examples of specific humidity profiles at Ny-Ålesund from radiosonde profiles (taken from the IGRA product) and from spatially and temporally matched IASI (MetOp-A and MetOp-B) and AIRS retrievals. AIRS retrievals are taken from both the Standard and the Support Product. The times indicated above each panel refer to the radiosonde launch time.

Two versions of the radiosonde data from Ny-Ålesund are available: high-resolution radiosonde profiles, and the radiosonde product by the Integrated Global Radiosonde Archive (IGRA). We choose to also use the IGRA product because a number of studies in literature obtains moisture inversion statistics from IGRA radiosonde products (e.g. Nygård et al., 2013, 2014; Naakka et al., 2018). At the same time, high-resolution radiosoundings might convey more information on Arctic moisture inversions. Thus in the present study, we compare them to the IGRA data set to assess possible discrepancies in inversion statistics.

The high-resolution radiosoundings used in this study were obtained from the Global Climate Observing System (GCOS) Reference Upper-Air Network (GRUAN; Seidel et al., 2009) and the Alfred Wegener Institute (AWI), which provides the radiosonde files on the PANGAEA portal (Maturilli, 2020). GRUAN was implemented to provide homogeneous high-quality reference observations, and GRUAN radiosonde data in particular are corrected in order to account for known sensor errors (Seidel et al., 2009). The GRUAN processing for Vaisala RS92 is discussed in detail in Dirksen et al. (2014). However, GRUAN currently supports a limited number of radiosonde models. For this reason, the GRUAN product for Ny-Ålesund is only available until 31st March 2017, when AWIPEV switched from Vaisala RS92 radiosondes to Vaisala RS41 radiosondes. Radiosonde data for the period 1st April 2017 to 31st December 2017 is provided on the PANGAEA portal by Maturilli (2020). Said data consists of high-resolution soundings, processed with the manufacturer software and checked against outliers. The radiosonde data from GRUAN and PANGAEA will be henceforth referred to as high-resolution radiosondes.



	pressure levels of retrieval (hPa)									
IASI	1100	1071	1042	1014	986	959	932	905	879	853
and	827	802	778	754	730	707	684	661	639	618
AIRS Support	596	576	555	535	516	497	478	460	442	424
	407									
AIRS Standard	1100	1000	925	850	700	600	500	400		
ERA5	1000	975	950	925	900	875	850	825	800	775
	750	700	650	600	550	500	450	400		

Table 1. Pressure levels (hPa) of the satellite and reanalysis products used in this study: IASI Level 2 Product, AIRS Level 2 Support Product, AIRS Level 2 Standard Product, and ERA5. Only levels below the 400-hPa level are reported.

The IGRA database consists of quality-assured profiles of several variables obtained from radiosoundings from several sites around the globe. Such profiles are interpolated on the mandatory pressure levels specified by the World Meteorological Organization (WMO): 1000, 925, 850, 700, 500, 400 and 300 hPa. If a profile strongly deviates from linearity between any consecutive levels, additional levels are included in the interpolation to better represent the non-linear behavior (Durre et al., 2006; Durre and Yin, 2008).

IGRA radiosoundings provide dew-point depression, while GRUAN and PANGAEA radiosoundings provide relative humidity. These quantities are all converted to specific humidity, using the formula for water vapor equilibrium pressure by Murphy and Koop (2005, eq. 10).

2.2 IASI: instrument and retrieval scheme

The Infrared Atmospheric Sounding Interferometer (IASI) was designed to provide accurate retrievals of temperature and humidity profiles, as well as total column trace gas concentrations. The primary goal of the IASI mission is to provide such profiles with high resolution and accuracy for assimilation in numerical weather prediction (Blumstein et al., 2004). The nominal accuracy of IASI water vapor retrievals is 10 % per 1-km-deep layer in the lower troposphere (Blumstein et al., 2004).

IASI is a Fourier transform infrared (FTIR) spectrometer. It covers the spectral range from 645 to 2760 cm^{-1} (3.62 to 15.5 μm), with a constant sampling interval of 0.25 cm^{-1} . This results in 8461 channels with a spectral resolution ranging between 0.35 and 0.5 cm^{-1} . IASI instruments are flown on board the three MetOp platforms which orbit the Earth on near-circular sun-synchronous polar low Earth orbits (LEOs) at an average altitude of 840 km. The orbits cross the equator northwards (ascending node) at 9.30 p.m.. IASI scans are cross-track, from -47.85° to $+47.85^\circ$, performed with rapid movements between 30 different viewing positions, spaced by 3.3° . The swath width is thus approximately 2000 km. The 3.3° instantaneous field of view is analyzed by a matrix of 2×2 circular cells, each corresponding to a 12-km-diameter circular pixel at nadir. Every scanning cycle includes a calibration, performed by observing cold space and an internal black body (Blumstein et al., 2004).

Aboard MetOp are also the Advanced Microwave Sounding Unit-A (AMSU-A), the Microwave Humidity Sounder (MHS), and the Advanced Very-High-Resolution Radiometer (AVHRR), which are coordinated with IASI to observe the same scene.



Measurements from these three instruments are used, alongside IASI spectra, in the IASI retrieval scheme (EUMETSAT, 2017). AMSU-A measures microwave radiances across 15 channels: 12 out of the 15 channels are located in the vicinity of the 55 GHz O₂ line, while the remaining channels are in atmospheric windows, at 23.8, 31.4, and 89 GHz (Mo, 1996). MHS
170 measures radiances across 5 channels, 3 of which are located in the 183.3 GHz H₂O line, while the rest are window channels at 89 and 150 GHz (NOAA, 2009). The AVHRR features 6 channels, in the visible, near infrared, and infrared windows, and is characterized by a very high resolution, with pixels of size 1.1 km (NOAA, 2009). In the IASI retrieval scheme AVHRR is only used for cloud detection (EUMETSAT, 2017).

The product employed in this study is the IASI Level 2 Product (PPF version 6.5) (EUMETSAT, 2017). The IASI Level 2
175 product provides specific humidity retrievals on 101 pressure levels. See Table 1 for a list of the pressure levels of the product.

The IASI retrieval scheme is composed of two major steps: a statistical all-sky regression-based retrieval, followed by a retrieval based on optimal estimation theory (Rodgers, 2000). The statistical retrieval, the Piece-Wise Linear Regression (PWL, see Hultberg and August (2014) for details) exploits microwave radiances from AMSU-A and MHS, as well as a limited number of IASI radiances principal components (PCs), to produce an accurate retrieval of temperature and humidity
180 profiles, as well as trace gas concentrations, under any sky condition. The statistical retrieval is then followed by an optimal estimation retrieval, based on IASI spectra, which employs the result of the PWL retrieval as first guess (EUMETSAT, 2017). See also Rodgers (2000) for an in-depth description of optimal estimation theory.

The optimal estimation retrieval is attempted for a given pixel if at least one of the following conditions is satisfied:

- no clouds,
- 185 – ECA (Effective Cloud Amount) < 25 %,
- CTP (Cloud Top Pressure) > 750 hPa.

Cloud information is obtained from IASI and AVHRR radiances, and from numerical weather prediction data. Because of these conditions on cloud cover, the optimal estimation retrieval that fully exploits IASI spectra is not always available (EUMETSAT, 2017).

190 It needs to be stressed that, despite the high number of vertical levels, the actual resolution is far lower, as the water vapor retrieval can contain a maximum of 8 independent pieces of information (EUMETSAT, 2017). Ebell et al. (2013) found from simulated IASI measurements that at a mid-latitude site, for example, IASI water vapor retrievals provide a number of degrees of freedom for signal that ranges between 2.5 and 7.2.

IASI water vapor retrievals have been widely validated, also at high latitudes (e.g. Kwon et al., 2012; August et al., 2012).
195 The most recent validation report by EUMETSAT shows a root mean square difference (RMSD) between IASI water vapor retrievals and co-located radiosoundings of approximately 0.3 g kg⁻¹ in the lower troposphere, averaged across the whole region above 60° latitude, in the period 01/02/2018 to 13/02/2018 (EUMETSAT, 2018).



2.3 AIRS: instrument and retrieval scheme

The Atmospheric Infrared Sounder (AIRS) is an infrared spectrometer, whose primary purpose, similarly to IASI, is to obtain temperature and humidity soundings for numerical weather prediction and climate studies (Parkinson, 2003). The accuracy for the AIRS water vapor retrievals has been estimated to be 15 % per 2-km-thick layer in the lower troposphere (Divakarla et al., 2006).

AIRS is a grating spectrometer that measures infrared spectra across 2378 channels, providing spectral coverage in 3 distinct spectral intervals: 650 to 1136 cm^{-1} (8.80 to 15.38 μm), 1216 to 1613 cm^{-1} (6.20 to 8.22 μm), and 2170 to 2674 cm^{-1} (3.74 to 4.61 μm). The nominal spectral resolution is $\lambda/\Delta\lambda = 1200$, while the spectral sampling is $\lambda/\Delta\lambda = 2400$. AIRS also includes four visible and near-infrared channels, with a higher spatial resolution (Aumann et al., 2003). The only AIRS instrument ever produced is flown on board the Aqua satellite, orbiting the Earth on a polar sun-synchronous LEO, at an average altitude of 705 km, crossing the equator northwards (ascending node) at 1.30 p.m. (Parkinson, 2003).

AIRS performs cross-track scans, with a swath width of 99°, corresponding to approximately 1650 km on Earth's surface. During each scan cycle, the entire swath is analyzed in 90 1.1°-wide FoVs, each corresponding to a 13.5-km-radius circular pixel at nadir. Similarly to IASI, each scan cycle includes a calibration procedure, by views of cold space and an internal black body (Aumann et al., 2003).

The products employed in this study are the AIRS Version 6 Level 2 Standard Product, and AIRS Version 6 Level 2 Support Product (Olsen et al., 2017a). The AIRS Level 2 Standard Product provides water vapor mixing ratio retrievals on 12 pressure levels, while the AIRS Level 2 Support Product provides water vapor mixing ratio retrievals on 100 pressure levels (see Table 1 for a list of the pressure levels of the different products).

Currently, AIRS retrievals only include infrared spectra from AIRS itself, and no microwave radiances (Susskind et al., 2019). The retrieval methodology employed by the AIRS science team is fundamentally different from that used for IASI: it involves a cloud-clearing procedure, followed by a physical retrieval that provides profiles of temperature, water vapor mixing ratio, and ozone, carbon monoxide and methane concentration profiles (Olsen et al., 2017b). AIRS FoVs are arranged into 3×3 arrays, named fields of regard (FoRs). Cloud-clearing requires the assumption that retrieved physical quantities in clear portions of the different FoVs belonging to the same FoR are the same. Details on the cloud-clearing procedure can be found in Susskind et al. (2003).

Once the radiances are cloud-cleared, the mentioned physical quantities are retrieved. As a consequence of the assumptions of the cloud-clearing procedure, one retrieval is performed for each FoR. Different quantities are retrieved sequentially, by finding the solution that best matches the radiances for select sets of channels. The first guess profile used as input is obtained from a neural network that processes AIRS radiances (Susskind et al., 2003; Olsen et al., 2017a, b).

AIRS retrievals are available on two different vertical grids: the AIRS Standard Product provides profiles on a limited number of levels (1100, 1000, 925, 850, 700, 600, 500, 400 hPa and above), while the AIRS Support Product provides retrievals on 100 pressure levels (31 of which are between 1100 and 400 hPa). Despite the higher number of levels, profiles contained within the Level 2 Support Product do not provide increased information content (Olsen et al., 2017b). However, we choose to analyze



both products, as the lower number of levels in the Standard Product might lead to a different representation of inversion characteristics compared to the Support Product. An example of this is shown in Fig. 1c, where an inversion is present in the AIRS Support Product sounding, but is absent in the specific humidity profile from the AIRS Standard Product.

235 AIRS water vapor products have been widely validated, also at high latitudes (e.g. Divakarla et al., 2006; Gettelman et al., 2006). The validation study by Divakarla et al. (2006) showed a 20 % to 30 % RMSD between AIRS water vapor retrievals at high latitudes in the lower troposphere and co-located radiosoundings.

A substantial difference between IASI retrievals and AIRS retrievals is the availability of AIRS retrievals under most sky conditions. As already explained, AIRS radiances are cloud-cleared, and its retrievals are thus available for most pixels in a given scene. However a quality control flag is assigned to each level of the retrievals. All levels in the retrievals with the lowest quality control score are here ignored, as recommended by the AIRS science team (Olsen et al., 2017b). On the other hand, IASI retrievals are available under specific sky conditions only as explained in section 2.2. No quality control is provided. Thus any pixel for which an optimal estimation retrieval is available is considered.

245 Note that, while the two instruments have FoVs of similar sizes, the spatial resolution at nadir of the IASI retrievals is 12 km, while that of AIRS retrievals is 49 km. While one retrieval is performed individually in each FoV of the IASI observations, in AIRS data one retrieval is performed per array of 3×3 FoVs, or FoR, as a result of the application of the cloud clearing procedure.

2.4 ERA5

250 Reanalyses assimilate atmospheric data from several data sets to provide an accurate and consistent numerical description of the atmospheric state. This coherent representation of atmospheric fields has significant applications in many fields in atmospheric sciences, and the fundamental role of reanalyses in climate monitoring applications is widely recognized.

In this study we choose to assess the performance of the ERA5 reanalysis (Hersbach et al., 2019) to capture moisture inversions. ERA5 is the latest reanalysis developed by ECMWF and is the successor of ERA-Interim (Berrisford et al., 2011). Older reanalyses, including ERA-Interim, have been found to show some limitations in representing Arctic moisture inversions (Brunke et al., 2015; Naakka et al., 2018). ERA5 has shown substantial improvements when compared to ERA-Interim and other older reanalyses in several respects (e.g. Graham et al., 2019). Thus, one of the objectives of this study is to perform inversion statistics also on ERA5 fields and compare them with statistics from radiosondes.

260 ERA5 was produced using 4D-Var assimilation on 137 model levels in the vertical on a reduced Gaussian grid with a resolution of 31 km (Hersbach et al., 2020). The product employed in this study is hourly, interpolated on 37 pressure levels, and on a regular latitude/longitude grid, with a resolution of 0.25° (see Table 1 for a list of the pressure levels that the product provides). The quantities contained in this product are to be thought as instantaneous and only representative of the grid-point they are associated to instead of a grid cell (ECMWF, 2017). ERA5 data was obtained from the Copernicus Climate Change Service (C3S) (2017).



It needs to be noted that the radiosondes launched from Ny-Ålesund are assimilated in the ERA5 reanalysis, which is also
265 the case for ERA-Interim. Thus, ERA5 performance could be substantially better in the Ny-Ålesund area than over regions
where no radiosondes are available for assimilation.

3 Methods

3.1 Inversion detection and inversion statistics

In literature many definitions of a moisture inversion were used (e.g. Devasthale et al., 2011; Naakka et al., 2018). In this study,
270 a moisture inversion is defined as a layer in the troposphere where specific humidity increases with height. It is thus delimited
by an inversion base level and an inversion top level. Two inversion layers in the same profile are considered as one if the
decrease in specific humidity between the two layers is $< 5\%$ the value of specific humidity at the top of the lower inversion.
Only moisture inversions below the 400-hPa level are considered, as this is the region of the atmosphere of interest for most
cloud processes, moisture transport events and modifications in downward longwave radiation by water vapor.

275 Moisture inversions are characterized through several parameters including frequency of occurrence, inversion depth, num-
ber of inversions in the same profile, inversion strength, and fraction of profiles containing surface-based inversions. Inversion
strength is here defined as the difference between specific humidity at inversion top and at inversion base. When computing
the fraction of profiles containing surface-based inversions, an inversion is considered surface-based if its base is below the
950-hPa level.

280 Moisture inversion statistics are also analyzed as functions of height, i.e. here pressure levels. Values of inversion frequency
of occurrence and median and quantiles of inversion strength and relative strength are analyzed in 100-hPa-deep layers, between
1000 hPa and 400 hPa. The frequency of occurrence in a given 100-hPa-deep layer is computed by counting how many profiles
contain a moisture inversion located, at least partially in that layer, and dividing by the total number of available profiles.
Inversion strength quantiles in a 100-hPa-deep layer are computed by performing the quantile across all inversions that are
285 detected in that layer. If more than one inversion is present in the same layer in a given profile, only the strongest is considered.
Relative inversion strength is computed by dividing the absolute value of inversion strength by the maximum value of specific
humidity across the inversion.

Profiles from high-resolution radiosondes undergo a further step: they are interpolated on a common vertical grid first with
levels spaced by 5 hPa. Additionally, inversions whose strength is lower than the measurement uncertainty are ignored. This is
290 done because these profiles, having an extremely high resolution, need to be filtered for small vertical fluctuations in specific
humidity. Measurement uncertainty for specific humidity is obtained with standard error propagation from the measurement
uncertainties declared by the manufacturer.



3.2 Reducing the vertical resolution of the radiosonde data

In order to assess how sensitive inversion statistics are to the vertical grid used and to perform a consistent comparison between
295 radiosondes and the other data sets, the vertical resolution of the radiosonde profiles is reduced to the corresponding vertical
grids of the different products. This coarsening is performed by linearly interpolating the radiosonde profiles on a vertical grid
with levels spaced by 5 hPa and then averaging the values of specific humidity in the interpolation across intervals centered on
the levels of the lower-resolved vertical grids.

3.3 Coincidence criteria

300 In order to compare statistics from radiosondes to statistics from ERA5, and IASI and AIRS retrievals, radiosondes need to be
matched with the profiles from the other data sets.

When comparing radiosondes to ERA5 fields, inversion statistics are performed on the grid-point that is closest to Ny-
Ålesund. The spread of the statistics across all grid-points within 31 km of Ny-Ålesund is also evaluated with 31 km being the
original horizontal model-grid spacing of ERA5.

305 For IASI, a satellite pixel is selected based on the following criteria:

- the measurement was performed within 1 hour before or after the radiosonde launch;
- the pixel is within 100 km of Ny-Ålesund;
- the lowest level of the retrievals is below the 970-hPa level
- the optimal estimation retrieval is available.

310 Among all pixels that satisfy these conditions, the closest one to Ny-Ålesund is selected. The third condition is included to
remove all pixels that fall on portions of the Spitzbergen island with complex topography, which might render the sounding
less reliable, especially at levels close to the surface.

When selecting the corresponding AIRS pixel, the time, distance and lowest pressure level criteria are the same as for IASI.
The closest pixel that satisfies these conditions and has quality flag 0 (best quality) or 1 (good quality) at the 925-hPa level is
315 chosen. If no such pixel is available, the closest pixel with quality flags 0 or 1 at any level below the 400-hPa level is chosen. In
both cases, levels with quality flag 2, which the AIRS science team recommends not to use (Olsen et al., 2017b), are ignored.

4 Results

4.1 Long-term characterization of moisture inversions at Ny-Ålesund from radiosondes

Table 2 shows the number of radiosondes launched during the study periods: January 2007 to December 2017, and 2017 only.
320 A high number of radiosondes is available for summer and autumn 2017, as measurement campaigns took place, where more
than one radiosonde was launched per day. For the long-term characterization of moisture inversions in Ny-Ålesund we only



	Total	DJF	MAM	JJA	SON
2007-2017	3855	953	954	969	979
2017	467	87	82	158	140

Table 2. Number of radiosondes available in the IGRA database for Ny-Ålesund during the 2007-2017 period, and 2017 only. Total number and the number per season are indicated. Only radiosondes launched at 12 UTC are included for the period 2007-2017, while all available radiosondes are included in the year 2017.

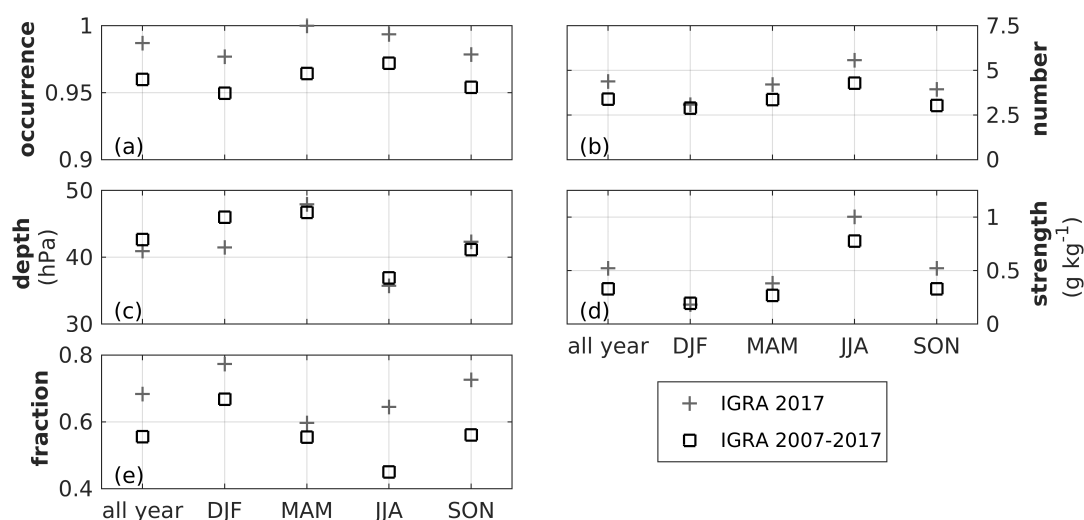


Figure 2. Statistics of moisture inversion parameters from IGRA radiosoundings at Ny-Ålesund for 2007-2017 and for 2017 only. The parameters included are (a) frequency of occurrence, (b) mean number of simultaneous inversions in the same profile, (c) mean depth of the strongest inversion in a profile, (d) mean strength of strongest inversion in a profile, and (e) fraction of soundings containing inversions with base below the 950-hPa level.

selected radiosondes launched at 12 UTC, while for the comparison with satellite and reanalysis products all radiosondes launched in 2017 were used.

Moisture inversion statistics from radiosondes show that moisture inversions were extremely frequent in the 2007-2017 analysis period, with a frequency of occurrence approximately constant and above 95 % in all seasons in the IGRA data set (Fig. 2a). Moisture inversions are often present on several levels simultaneously with a mean number of 3.4 for the whole time period and 2.9 (4.3) inversion layers in winter (summer). Overall, 82.3 % of all soundings featured more than one moisture inversion layer. Surface-based moisture inversions, i.e. inversions with a base below the 950-hPa level, are found in 42.6 % of the profiles (Fig. 2e). Furthermore, a clear seasonal cycle is present in some of the inversion characteristics: moisture inversions are deeper in winter (45 hPa) than in summer (35 hPa). Also, surface-based inversions occur more frequently in winter (51.1 %) than in summer (33.7 %). However, inversion strength is larger in summer than in winter. As expected from the higher water

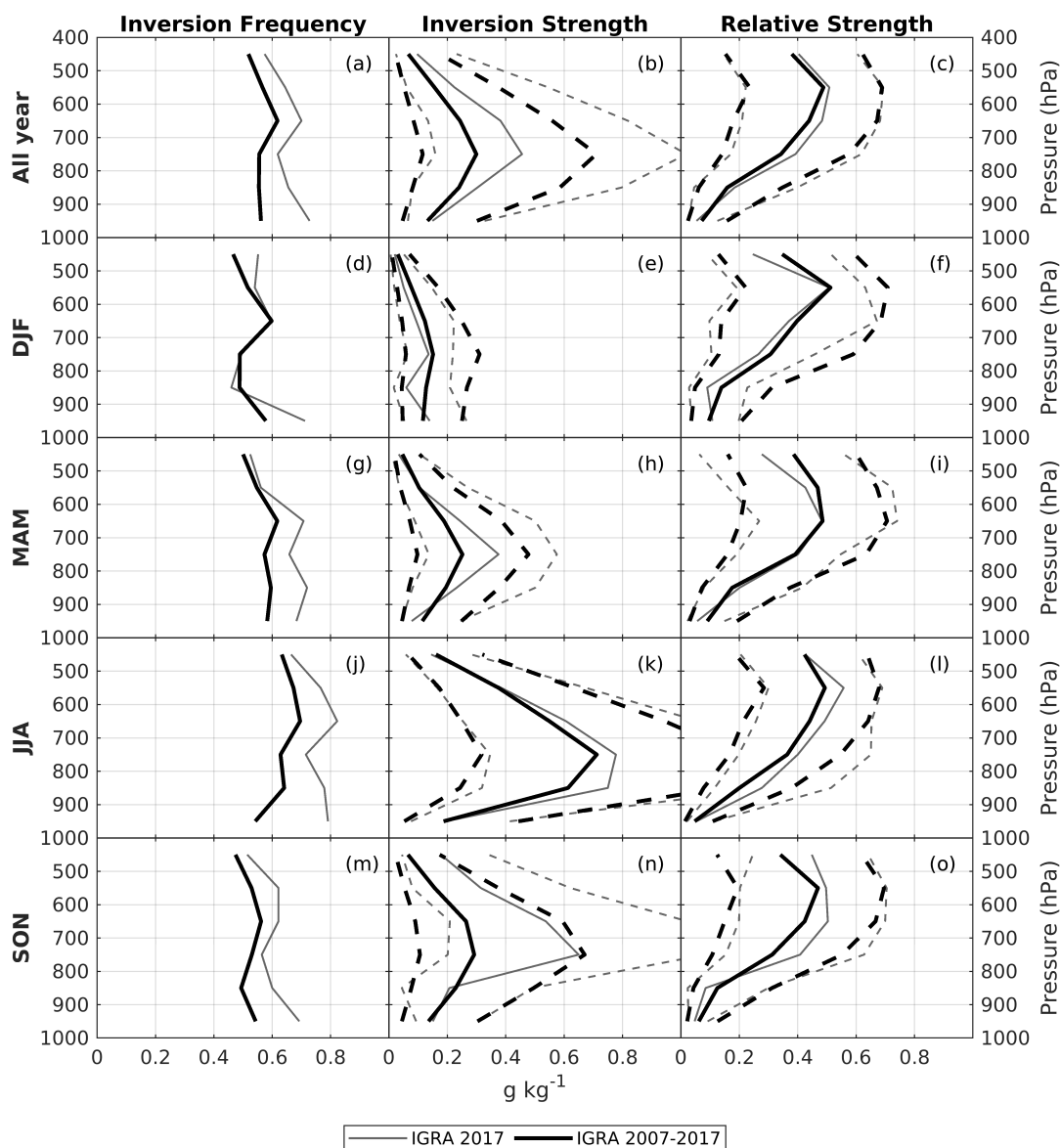


Figure 3. Moisture inversion frequency (left), strength (middle), and relative strength (right) computed in 100-hPa-deep layers from 1000 hPa to 400 hPa from IGRA radiosondes at Ny-Ålesund for the year 2017 and for the 2007-2017 period. Solid lines in the strength panels indicate the median value. Dashed lines indicate the 0.25 and 0.75 quantiles of strength and relative strength.

vapor content in summer, moisture inversions are stronger in this season in absolute values, with a median inversion strength of the strongest inversion in the profile of 0.78 g kg^{-1} , while the value in winter is less than 0.18 g kg^{-1} .

The results shown in Fig. 2 are consistent with those by Nygård et al. (2014), who performed a similar analysis for different
 335 Arctic sites including Ny-Ålesund and employing IGRA radiosondes for the 2000-2009 period.



Fig. 3 shows the dependency of inversion frequency of occurrence, strength, and relative strength on height. These parameters are computed for 100-hPa-deep layers from 1000 hPa up to 400 hPa. The all-year inversion frequency profile (Fig. 3a) displays a rather vertically constant inversion frequency of approximately 60 % in the long-term data set. Some vertical variability in inversion frequency is observed in the different seasons, especially in winter and summer. The winter profile (Fig. 3d) shows in fact two maxima close to 60 %, at the surface and in the 700-to-600-hPa layer. In summer (Fig. 3j), inversion frequency increases with height, from 50 % at the surface to above 60 % above the 700-hPa level. Inversion frequency in summer is higher than that in winter, at any level, except in the lowest layer (1000 to 900 hPa).

The second column in Fig. 3 shows median inversion strength computed as a function of pressure in 100-hPa-deep layers, 0.25 and 0.75 quantiles are also shown. Inversion strength in winter (Fig. 3e) is approximately constant with height from the surface up to the 700-hPa level with a median value of approximately 0.15 g kg^{-1} . In this season, more than 75 % of the detected inversions have a strength lower than 0.3 g kg^{-1} , at any height. A distinguishable vertical maximum of median inversion strength can be observed in the other seasons with maximum values being located between 700 and 800 hPa in all seasons. The vertical distribution of inversion strength in summer (Fig. 3k) shows the highest vertical variability and the largest spread around the median value: median inversion strength ranges from 0.19 g kg^{-1} below the 900-hPa level to 0.71 g kg^{-1} between 700 and 800 hPa.

The third column in Fig. 3 shows the distribution of relative inversion strength, i.e. inversion strength divided by the value of specific humidity at inversion top. While absolute inversion strength displays a clear seasonality in its vertical distribution, the vertical distributions of normalized inversion strength are very similar across all seasons. This indicates that the observed seasonality in the vertical distribution of absolute inversion strength is a mere consequence of the higher moisture content in summer than in winter, and of the different vertical distributions of specific humidity across the year. The relative inversion strength typically increases from about 10 % in the lowest layer to about 50 % in the 600-to-500-hPa layer.

Figures 2 and 3 also show that data for the year 2017 alone display a higher number of inversions in spring, summer and autumn. The seasonal cycle of inversion occurrence is still similar compared to the long-term mean data set. Vertical distributions of inversion strength are close to the climatology in all seasons, except in autumn (Fig. 3n) above the 800-hPa level, when the strength was significantly higher than the 2007-2017 climatology.

4.2 Sensitivity analysis to the vertical grid

The reanalysis and satellite data sets evaluated in this study provide water vapor variables on different vertical grids, that are far lower resolved than radiosonde profiles. Since the usage of different vertical grids might already result in different inversion statistics, in this section, the sensitivity of the inversion statistics to the vertical grid resolution is assessed. The same metrics as shown in the previous section are provided for the 2017 IGRA radiosondes which have been adjusted to the vertical grids of the other data sets. Statistics from the high-resolution radiosondes from GRUAN and PANGAEA are also shown.

Note that the results for the radiosondes adjusted to the vertical grid of the IASI and AIRS Support retrievals are reported for completeness. Note again that the actual resolution of the retrieved profiles of the satellite instruments is far lower than the number of levels of the products. Additionally, each retrieval has a different number of independent pieces of information with

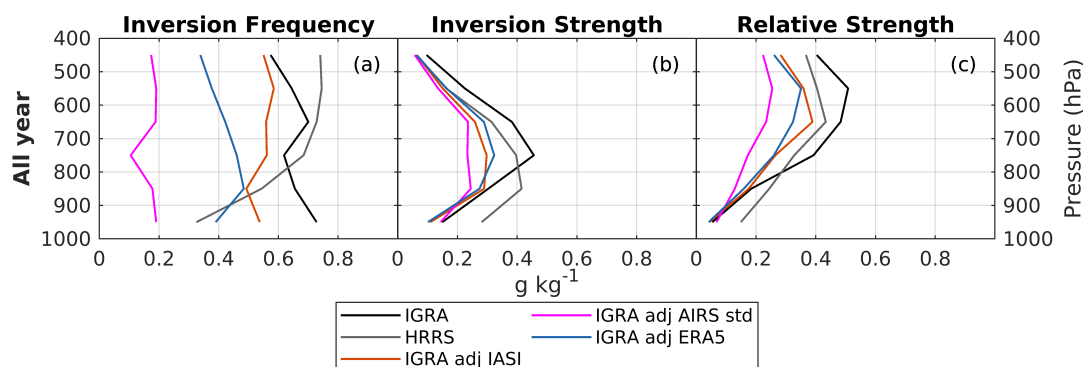


Figure 4. (a) Moisture inversion frequency, (b) median strength, and (c) median relative strength computed in 100-hPa-deep layers from 1000 hPa to 400 hPa from IGRA radiosondes for the year 2017. The vertical grid of the radiosonde profiles have been adjusted to the same vertical grid of the other data sets analyzed in this study, i.e. IASI level 2 product, AIRS Standard Product, ERA5 reanalysis. Note that the vertical grid of the AIRS Support Product is the same as the IASI level 2 product. Statistics from the high-resolution radiosondes (HRRS) are also shown.

370 a different vertical distribution. A proper adjustment of the vertical resolution of the radiosondes to the true resolution of the satellite-based profiles would require obtaining the averaging kernels from the inversion algorithms for every retrieval. This is out of the scope of this study. We argue that radiosondes adjusted to the vertical grid of the AIRS Standard Product provide, nonetheless, a resolution that is qualitatively similar to that of the actual IASI and AIRS retrieval resolution. This is because the number of pressure levels available in the AIRS Standard Product (7 between 1000 and 400 hPa) is close to the typical number of degrees of freedom of the IASI retrievals (e.g., ranging between 2.5 and 7.2, according to Ebell et al. (2013)).

375 Similarly to Fig. 3, Fig. 4 shows statistics of inversion frequency of occurrence (panel a), strength (b), and relative strength (c), for the vertically adjusted IGRA radiosondes at Ny-Ålesund for 2017. Here, the effect of employing a lower-resolved vertical grid is particularly evident in the inversion frequency (Fig. 4a): the lower the grid resolution, the lower the inversion frequency.

380 Radiosondes adjusted to the ERA5 vertical grid show an inversion frequency that is 20 to 30 percentage points lower at any pressure level than that observed in the original IGRA radiosondes. Overall, inversions are in fact present in 73 % of profiles in winter and 91 % in summer in the radiosondes adjusted to the ERA5 vertical grid, while for the original IGRA radiosondes the same values are 92 % and 97 %, respectively (not shown).

Inversion frequency is even more reduced in the radiosondes adjusted to the vertical grid of the AIRS Standard Product: inversion frequency is below 20 % at any level and in any season and thus about 50 percentage points lower than that of the original IGRA data.

The median strength values below the 800-hPa level in all adjusted radiosondes show a very good agreement with those obtained from the original IGRA radiosondes at all resolutions (Fig. 4b). Strength seems to be underestimated above the 800-



Instrument	All in 2017	DJF	MAM	JJA	SON
MetOp-A IASI	228 (48.8 %)	46 (52.9 %)	41 (50.0 %)	69 (43.7 %)	72 (51.4 %)
MetOp-B IASI	219 (46.9 %)	34 (39.0 %)	43 (52.4 %)	76 (48.1 %)	66 (47.1 %)
AIRS	323 (69.2 %)	63 (72.4 %)	61 (74.4 %)	107 (67.7 %)	92 (65.7 %)

Table 3. Number of spatial and temporal matches between radiosondes at Ny-Ålesund and MetOp-A IASI, MetOp-B IASI, and AIRS retrievals in 2017. Total number of matches and the number per season are shown. Coincidence criteria are explained in section 3.3. Values in parentheses indicate the ratio of the number of coincidences and the number of available radiosondes.

Instrument	Mean distance	Mean time difference	Mean abs. time difference
MetOp-A IASI	47.6 km	2.9 min	25.7 min
MetOp-B IASI	47.3 km	4.3 min	26.9 min
AIRS	49.8 km	-12.9 min	26.2 min

Table 4. Mean distance from Ny-Ålesund, mean time difference, and mean absolute time difference between radiosonde launches in 2017 and IASI (MetOp-A and MetOp-B), and AIRS pixels matched with the radiosondes.

hPa level, especially between 800 and 600 hPa. The same conclusions apply to median relative strength profiles shown in
 390 Fig. 4c.

Fig. 4 also compares moisture inversion statistics from IGRA to statistics from high-resolution radiosondes. These statistics show some discrepancies, especially in terms of inversion frequency. Compared to high-resolution radiosondes, IGRA radiosondes seem to strongly overestimate inversion frequency below the 800-hPa level, and underestimate it above the 600-hPa level. We attribute the former to the conservative approach we used to obtain inversions from the high-resolution radiosondes:
 395 excluding inversions whose strength is below the measurement uncertainty on specific humidity has probably removed many inversions that are actually present in the IGRA data. This is further confirmed by the relative strength (Fig. 4c), as relative inversion strength is significantly higher in high-resolution radiosondes below the 800-hPa level compared to IGRA. The underestimation in occurrence in IGRA above the 600-hPa level can be attributed to the IGRA processing itself, which seems to remove weaker inversions that we still detected in the high-resolution radiosondes. This is indicated by the higher inversion
 400 strength in IGRA above this level. We thus conclude that IGRA profiles capture all relevant inversions below the 600-hPa level, with weak inversions not being detected above this level.

4.3 Infrared sounders: IASI and AIRS

In this section we assess the capability of IASI and AIRS retrievals to detect Arctic moisture inversions. Soundings from these instruments were matched with radiosondes using the coincidence criteria described in section 3.3. Table 3 shows the number
 405 of obtained matches. The number of available retrievals for both IASI instruments is approximately 50 % of the number of available radiosondes. At the same time, the number of available AIRS retrievals is approximately 70 % of the number of



available radiosondes. This difference between the instruments is attributable to cloud cover, as IASI retrievals are available only under specific sky conditions, while AIRS retrievals involve a cloud-clearing procedure (see sections 2.2 and 2.3).

410 Table 4 shows the average distances between Ny-Ålesund and the center of the IASI and AIRS pixels selected by the coincidence criteria. The mean distance for matched AIRS pixels is 49.8 km, which is very close to the AIRS field of regard dimension of 49 km. Even if the IASI pixel size is 12 km only, the average distance is still 47 km. This rather large difference for IASI is attributable to the issue of cloud contamination, as, in most pixels, the conditions on cloud cover required to perform the IASI optimal estimation retrieval are not satisfied.

415 Moisture inversions are found in 31.6 % (23.9 %) of IASI-A (IASI-B) soundings, which is distinctly lower than the 48.2 % frequency of occurrence observed in the IGRA radiosondes adjusted to the vertical grid of the AIRS Standard Product. The overall frequency of occurrence in the AIRS Support Product, i.e. 24.1 %, is underestimated as well. The frequency of occurrence in the AIRS Standard Product (11.4 %) is even lower. Additionally, in the vast majority of cases, no more than one inversion appears in the IASI and AIRS retrievals: two or more inversions are in fact observed only in 3.1 %, 0.9 %, 0 % and 0 % of all soundings matched with radiosondes for MetOp-A IASI, MetOp-B IASI, the AIRS Support Product and the AIRS
420 Standard Product, respectively.

Figure 5 shows profiles of inversion frequency, median strength and number of detected inversions as a function of height from IASI, AIRS and the IGRA radiosondes adjusted to the vertical grid of the AIRS Standard Product. In the third column the number of inversions in each layer in IASI and AIRS data is indicated, as, in many layers, median strength was computed out of an extremely low number of inversions, and thus is not statistically meaningful. Inversion frequency in IASI and AIRS retrievals
425 is in general distinctly lower in all seasons and at most pressure levels than the one observed in the radiosondes. Exception to this is IASI-A in winter and autumn below the 800-hPa level. Here MetOp-A IASI displays an inversion frequency in general comparable to that observed in the radiosondes adjusted to the AIRS Standard Product grid. Interestingly, in the lowest pressure layer in winter, the inversion frequency from IASI MetOp-A product (33 %) is higher than that obtained from the adjusted radiosondes (Fig. 5d). The IASI product based on MetOp-B displays a similar performance compared to the one
430 based on IASI-A, except below the 800-hPa level in autumn and winter, where the frequency of occurrence is lower (11 % in winter). In winter, both IASI products from MetOp-A and -B capture roughly the vertical distribution of inversion frequency with a maximum in the lowest pressure layer. Fig. 5 shows that inversion frequency from AIRS retrievals is close to or lower than that from IASI retrievals, except from the levels between 900 and 600 hPa in summer. Furthermore, neither AIRS products detected any inversions in winter below the 700-hPa level. Inversion frequency in the AIRS Standard Product is in general lower
435 than the one in the AIRS Support Product at any level. This indicates that, while nominally the information content of the two products should be the same, the AIRS Support Product seems to be more suited to study moisture inversions.

The second column in Fig. 5 shows profiles of median inversion strength in 100-hPa-deep layers from IASI, AIRS and radiosondes adjusted to the AIRS Standard Product grid. Since not enough inversions are available to perform a meaningful statistic of inversion strength for single seasons (Fig. 5, third column), we will comment on the all-year strength statistic only
440 (Fig. 5b). Inversion strength statistics for single seasons are included for completeness. The all-year statistic in Fig. 5b shows that median strength from IASI retrievals never rises above 0.1 g kg^{-1} . This is much lower than the observed inversion strength

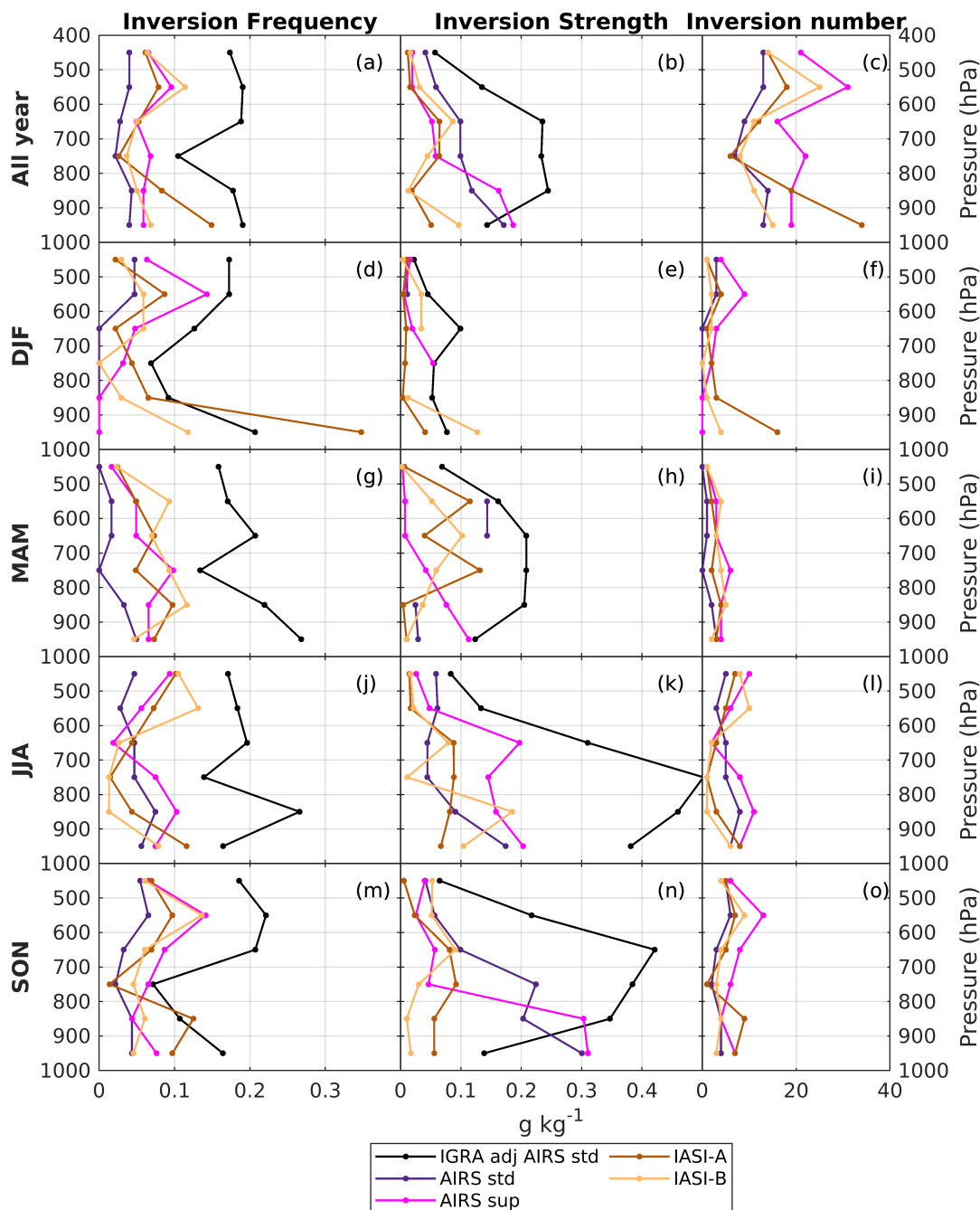


Figure 5. Moisture inversion frequency (left), median strength (middle), and number of detected inversions (right) in 100-hPa-deep layers from 1000 hPa to 400 hPa from IASI and AIRS retrievals and IGRA radiosondes at Ny-Ålesund for the year 2017. Satellite data includes the IASI level 2 product from MetOp-A IASI and MetOp-B IASI, the AIRS Support Product and the AIRS Standard Product. The vertical resolution of the IGRA radiosonde profiles have been adjusted to the vertical grid of the AIRS Standard Product.



based on the adjusted radiosondes with values of about 0.25 g kg^{-1} between 900 and 600 hPa. IASI soundings thus strongly underestimate moisture inversion strength at all heights. The strong underestimation of inversion strength can also be seen in the AIRS products in particular between 800 and 400 hPa. Both AIRS products seem to better represent the inversion strength
445 below the 800-hPa level. The all-year median strength below the 900-hPa level from both AIRS products is in fact close to the value of the adjusted radiosondes.

The analysis performed in this section clearly demonstrates that both IASI and AIRS retrievals have strong limitations when it comes to detecting complex features in a specific humidity profile such as inversions. Even in comparison to radiosonde data with a rather coarse vertical resolution, the frequency of occurrence of moisture inversions is by far underestimated by the
450 satellite products. This is most likely due to the low vertical humidity information from the passive sensors and the resulting smoothed humidity profiles. IASI seems to be able to capture better inversion frequency below the 800-hPa level in winter. Surprisingly, the frequency of occurrence of inversions from IASI-A data in winter below the 900-hPa level is triple the value in IASI-B data. While AIRS detected less inversions than IASI in the study period, it better portrayed their strength, especially below the 800-hPa level.

455 4.4 ERA5

In this section the results obtained from ERA5 will be shown and compared to those from radiosondes for the year 2017. Inversion statistics are obtained for the grid-point that is closest to Ny-Ålesund, and for all grid-points within 31 km of Ny-Ålesund. Information on the spread of the statistics across these grid-points is obtained by computing the median and 0.25 and 0.75 quantiles of the parameters computed for the single grid-points. Inversion statistics from the reanalysis are compared to
460 statistics from radiosondes adjusted to the ERA5 vertical grid to enable a fairer comparison.

In ERA5, we find moisture inversions in 71.9 % of the time in winter and 82.3 % of the time in summer when analyzing profiles from the grid-point closest to Ny-Ålesund. Observed values based on IGRA radiosondes (adjusted to the ERA5 vertical resolution) are 75.9 % and 93.0 %, respectively, and are thus 4 to 10 percentage points higher than in the reanalysis. Profiles containing multiple inversions are observed 33.9 % of the time in ERA5, 22.5 % in winter and 35.4 % in summer. The same
465 values obtained from adjusted radiosondes are 56.5 %, 44.8 %, and 67.1 %, respectively. When calculating the median strength of the strongest inversion in each profile, we find larger discrepancies of about 50 %: while ERA5 shows values of 0.05 (0.22 g kg^{-1}) in winter (summer), we find 0.10 (0.49 g kg^{-1}) based on the adjusted radiosonde data.

Fig. 6 shows the vertical distribution of inversion frequency and median strength in ERA5 profiles and in radiosondes, both in their original resolution, and adjusted to the ERA5 vertical grid. At any height, and in any season, ERA5 underestimates
470 inversion frequency by 10 to 20 percentage points, except below the 800-hPa level in winter, and below the 900-hPa level in summer, where inversion frequency in ERA5 is very close to that from the adjusted radiosondes. In autumn, below the 900-hPa level, inversion frequency is overestimated by approximately 10 percentage points. In general, ERA5 captures the vertical distribution of moisture inversion frequency well even though with lower values. Note however that inversion frequency in the ERA5 data is distinctly lower than the one based on the original IGRA radiosondes. This underlines once more that for a
475 consistent comparison the impact of the vertical grid needs to be taken into account.

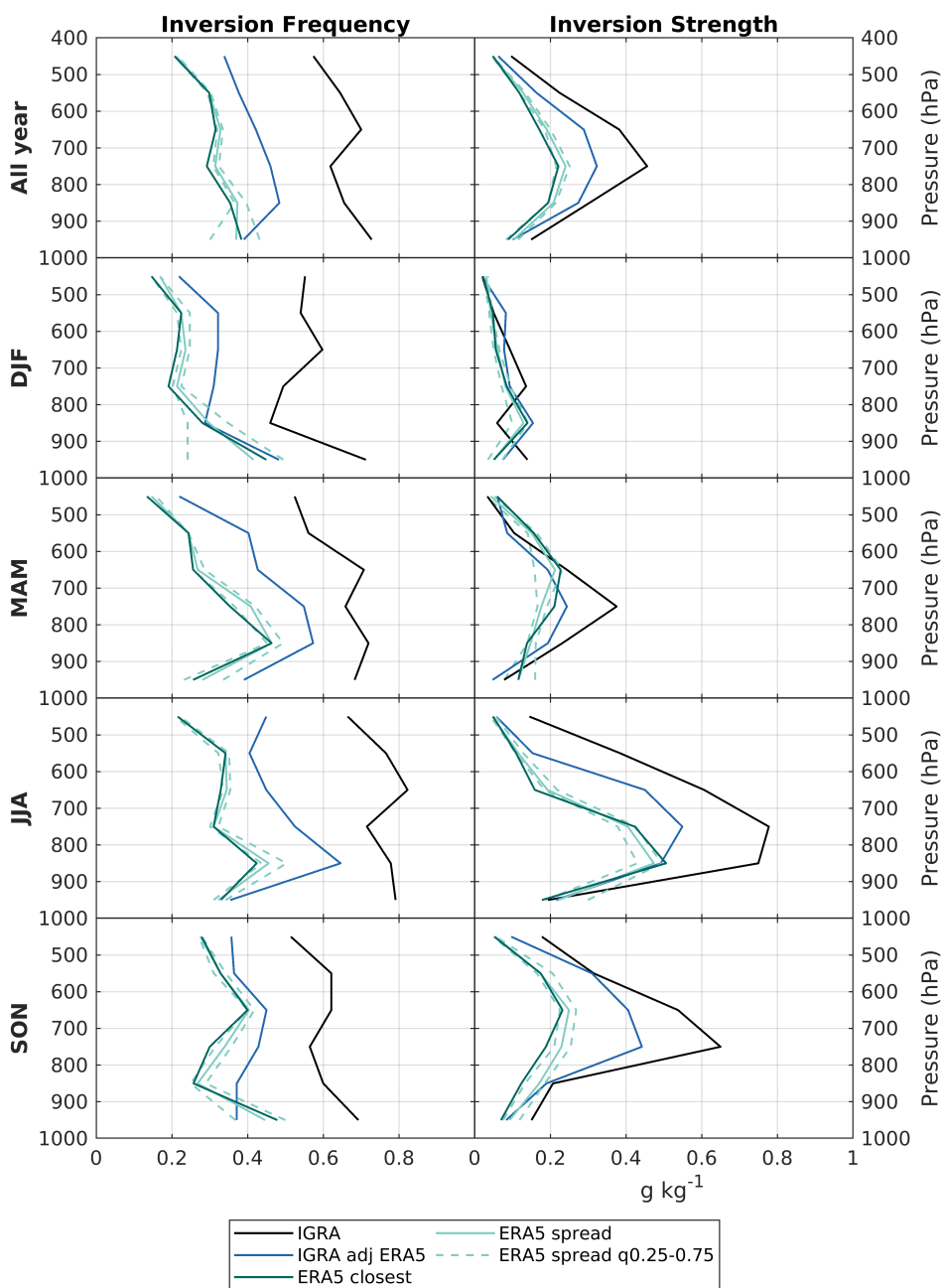


Figure 6. Moisture inversion frequency (left) and median strength (right) computed in 100-hPa-deep layers from 1000 hPa to 400 hPa from the ERA5 reanalysis fields and IGRA radiosondes at Ny-Ålesund for the year 2017 and for the different seasons in 2017. IGRA radiosonde profiles are included in their original vertical resolution and in the vertical resolution adjusted to the vertical grid of ERA5. ERA5 closest indicates the statistics taken from the grid-point that is closest to Ny-Ålesund only. The distribution of the statistics from ERA5 across all grid-points within 31 km of Ny-Ålesund is also shown: displayed are the median value (ERA5 spread) and 0.25 and 0.75 quantiles (ERA5 spread q0.25-0.75).



A similar analysis was performed by Naakka et al. (2018) for the ERA-Interim reanalysis: they found that when comparing ERA-Interim with IGRA radiosondes (in their original resolution), inversion frequency is underestimated by ERA-Interim at all height levels by approximately 15 and 30 percentage points in winter and up to 40 percentage points in summer in the North Atlantic region (Naakka et al., 2018, Fig. 7c-d). Also for ERA5, we see an underestimation of moisture inversion frequency in the same order of magnitude when comparing the reanalysis to the original IGRA radiosounding data at Ny-Ålesund (Fig. 6, left column). This indicates a similar performance of both reanalyses in capturing the frequency of occurrence of moisture inversions. However, a more thorough comparison of both reanalyses would be needed in order to conclude if and which reanalysis might show a better skill in representing moisture inversion frequency.

Fig. 6 also shows that the spread in the inversion frequency profiles across the considered ERA5 grid-points is low, except below the 800-hPa level in winter (panel c). Results are thus not strongly depending on the chosen ERA5 grid box and indicate a robust feature. The higher spatial variability below the 800-hPa level in winter could be an actual characteristic of moisture inversions in the Ny-Ålesund region, which might be due to the complex topography and the presence of several surface types (sea, sea ice, glaciers, snow cover, and bare land surfaces).

When looking at the profiles of median inversion strength (Fig. 6, right column), we find a very good agreement between ERA5 and the adjusted radiosondes for winter and spring. Conversely, median inversion strength is strongly underestimated in summer between 600 and 800 hPa (by 23 % between 800 and 700 hPa, and 65 % between 700 and 600 hPa compared to adjusted radiosondes), and in autumn between 800 and 500 hPa (with a maximum underestimation of 57 % between 800 and 700 hPa). These are also the pressure layers where maximum median inversion strength is observed in the radiosondes. Also for inversion strength, there is a negligible spread between profiles obtained from different ERA5 grid-points, indicating that the found model features occur also in the surrounding grid-points and thus are robust. In contrast to Chang et al. (2021), we do not observe a distinct underestimation in occurrence and strength of surface-based inversions in ERA5. However, this might also be a result of the different vertical resolutions of the radiosonde data used in the study.

In conclusion, ERA5 provides a good representation of the characteristics of moisture inversions above Ny-Ålesund, if its lower vertical resolution compared to radiosondes is taken into account. The agreement between the reanalysis and adjusted radiosondes is especially good in winter and spring. Least agreement is found in autumn.

5 Conclusions and Outlook

Moisture inversions are extremely frequent in the Arctic atmosphere. They are strongly intertwined with cloud processes, as well as the energy budget, by affecting the downward longwave radiation. Our knowledge of their characteristics is still limited because of the lack of *in situ* data in this region and because of uncertainties in moisture estimates from reanalyses and satellite products. In this study, the capability of two benchmark satellite sounders, the Infrared Atmospheric Sounding Interferometer (IASI) and the Atmospheric Infrared Sounder (AIRS), to detect moisture inversions at an Arctic site, Ny-Ålesund, is systematically assessed for the first time. Additionally, an accurate characterization of moisture inversions above Ny-Ålesund



is performed employing radiosonde data. The capability of the ERA5 reanalysis to detect Arctic moisture inversions has also been addressed. The most important findings of this study are as follows:

- 510 – Confirming results from previous studies, it has been shown that moisture inversions are extremely frequent above Ny-
Ålesund in the time period 2007-2017, based on radiosonde data. The frequency of occurrence is above 95 % across all
seasons. Moisture inversions often occur on several levels simultaneously (82 % of all soundings). IGRA radiosoundings
display an average of 2.9 simultaneous inversions in winter and 4.3 in summer. IGRA soundings highlight a strong
515 seasonal variability in the median strength of the strongest inversion in each profile, which ranges from 0.18 g kg⁻¹ in
winter to 0.78 g kg⁻¹ in summer. The vertical distribution of the frequency of occurrence of moisture inversions ranges
between 50 and 60 % in winter in all 100-hPa-deep layers between 1000 and 400 hPa. In this season, median inversion
strength in 100-hPa-deep layers is always lower than 0.15 g kg⁻¹. In summer, moisture inversion frequency ranges
between 60 and 70 % in each 100-hPa-deep layer above the 900-hPa level, with a value of 54 % between 1000 and 900
hPa. Summer median inversion strength in 100-hPa-deep layers peaks between 800 and 700 hPa, at 0.71 g kg⁻¹, while
520 its value in the lowest layer is 0.19 g kg⁻¹. Spring and autumn act as transition seasons, with most statistics displaying
values in between the winter and summer values. While the vertical distribution of the inversion strength clearly displays
a seasonal cycle with maximum values in summer, the vertical distribution of the relative strength (relative to the specific
humidity value at inversion top), does not change throughout the course of the year. This shows that the seasonal cycle
in inversion strength is merely a consequence of the annual cycle of moisture content.
- 525 – Moisture inversion statistics are strongly sensitive to the vertical grid of the specific humidity profile. This was demon-
strated by calculating inversion statistics based on radiosondes adjusted to the vertical grids of the other data sets used
in this study. Typically, the lower the vertical resolution, the lower the inversion frequency. It has been shown that the
vertical resolution of the ERA5 reanalysis is sufficient to capture most of the characteristics of moisture inversions ob-
served in the IGRA radiosondes, with an underestimation of inversion frequency of 20 to 30 percentage points in any
530 100-hPa-deep-layer. At the same time, vertical grids that include the WMO mandatory levels only, such as the vertical
grid of the AIRS Standard Product, do not provide a high enough resolution and the frequency of occurrence of moisture
inversions is dramatically underestimated (by about 50 percentage points). Inversion strength and relative strength seem
to be less sensitive to the resolution of the vertical grid: in particular in the lowest height levels, results are similar among
the different vertically regridted radiosonde data sets.
- 535 – When analyzing humidity profiles from IASI and AIRS retrievals, we found that moisture inversion characteristics are
quite different compared to the statistics based on IGRA radiosoundings. This is most likely due to both the coarsely
resolved vertical grid and the rather low vertical humidity information content of the passive remote sensing instruments.
This results in strongly vertically smoothed humidity profiles. While IGRA radiosoundings reveal that moisture inver-
sions are present 98.7 % of the time in 2017, for the MetOp-A IASI, the MetOp-B IASI, the AIRS Support and the AIRS
540 Standard Product, inversions are only found in 32 %, 24 %, 24 % and 11 % of the profiles, respectively. Inversion fre-
quency in 100-hPa-deep layers is below 10 % in most 100-hPa-deep layers and in most seasons for the retrievals from all



three instruments. These values are much lower than the ones for the IGRA radiosondes regridded to the AIRS Standard Product grid (10-20 %) and much lower than the values based on the original IGRA data (60-70 %). A notable exception has been found for the IASI data below the 900-hPa level and in particular for winter: here, the statistics from IASI show in fact an inversion frequency of 33 % (MetOp-A) and 11 % (MetOp-B) which are closer to the observed one (20 %). For both AIRS products, no inversions at all are detected below the 700-hPa level in winter. For all satellite products, inversion strength is strongly underestimated, in particular for the IASI retrievals. Both AIRS products better capture the inversion strength in the lowest layers, in particular below the 900-hPa level where AIRS reports median values of 0.17 and 0.19 g kg⁻¹ in the Support and Standard Products, respectively, while the value of the regridded radiosondes is 0.14 g kg⁻¹. Note however, that due to the low number of inversions that have been detected based on the satellite data, it is difficult to draw a final conclusion here.

– For 2017, ERA5 represents Arctic moisture inversion characteristics at Ny-Ålesund very well, if the lower vertical resolution of the reanalysis is taken into account. This holds in particular for the inversion frequency in the lowest pressure layer between 1000 and 900 hPa and in particular in winter. Regarding the all-year frequency of occurrence, ERA5 underestimates inversion frequency by about 12 percentage points at heights above the 900-hPa level. However, when comparing ERA5 to the IGRA data set in its original, i.e. higher, resolution, inversion frequency is underestimated throughout the atmospheric column by about 30 to 40 percentage points.

The comparison of inversion strength reveals a very good agreement between ERA5 and the adjusted radiosondes, with significant underestimations only in summer between 800 and 600 hPa (of 0.21 g kg⁻¹) and in autumn between 800 and 500 hPa (of 0.19 g kg⁻¹).

While the limitations of the retrievals from IASI and AIRS became clear from the analysis performed in this study, it has not been possible to characterize in more detail the inversions that the satellite retrievals do actually capture. A problem here is the low number of available samples as moisture inversions were present in a small fraction of the retrieved moisture profiles only. Performing such a characterization would thus require the analysis of several years of data and the inclusion of more radiosonde locations in the Arctic. In this way, the analysis of ERA5, which showed a good representation of moisture inversion characteristics at Ny-Ålesund, could also be extended for different locations. If ERA5 showed a similar good performance, the data could also be used as a reference to be compared to the satellite retrievals across the whole Arctic region.

Additionally, the effect of cloud cover on the satellite retrievals has not been assessed in this study. The IASI retrievals are performed only under specific sky conditions and the AIRS radiances are cloud-cleared. It would however be highly instructive to perform the same analysis for clear-sky cases only, in order to assess if the performance of the satellite retrievals improves. This would again require the analysis of several years of data as clouds occur frequently across the Arctic region.

In this regard, also the performance of microwave sounders alone could be assessed, as they have the advantage of being able to sense through cloud layers. Microwave radiances from MHS and AMSU-A aboard MetOp are already employed in the IASI retrieval scheme. Thus, a considerable fraction of the information contained in the IASI soundings could come



575 from the microwave radiances. Comparing inversion statistics from the IASI first guess retrieval, mostly based on microwave observations, to the statistics obtained in this study could provide further insights in the performance of the IASI retrievals.

Since radiosonde observations are commonly restricted to land areas only, detailed information about the thermodynamic structure of the atmosphere over the central Arctic is sparse. Here, campaign-based measurements from ships can provide more additional information. In this respect, the unique one-year observations of the Multidisciplinary drifting Observatory for
580 the Study of the Arctic Climate (MOSAiC) including operational radiosonde launches four times daily could provide further insights into the moisture inversion climatology over the Arctic.

Data availability. The IGRA radiosonde data for Ny-Ålesund are available at <https://www.ncei.noaa.gov/products/weather-balloon/integrated-global-radiosonde-archive>, radiosonde station code SVM00001004. High-resolution radiosonde data are available from GRUAN until March 2017 (Seidel et al. (2009); <https://www.gruan.org/data/file-archive>), and on PANGAEA from April 2017 onwards (Maturilli (2020); <https://doi.pangaea.de/10.1594/PANGAEA.914973>). IASI Level 2 data were downloaded using EUMETSAT's Data Centre Archive Ordering Application (<http://archive.eumetsat.int>). AIRS Level 2 Standard and Support products were obtained from NASA's GES DISC service (respectively https://disc.gsfc.nasa.gov/datasets/AIRS2RET_006/summary, and https://disc.gsfc.nasa.gov/datasets/AIRS2SUP_006/summary). ERA5 data were obtained from the Copernicus Climate Change Service (C3S) (2017) (<https://doi.org/10.24381/cds.bd0915c6>).

Author contributions. GC performed the analysis and visualization, with the supervision of KE. Both GC and KE contributed to the interpretation of the results and the writing of the manuscript.
590

Competing interests. The authors declare that they have no conflict of interest.

Acknowledgements. We gratefully acknowledge the funding by the Deutsche Forschungsgemeinschaft (DFG, German Research Foundation) – Project-ID 268020496 – TRR 172, within the Transregional Collaborative Research Center “Arctic Amplification: Climate Relevant Atmospheric and SurfaCe Processes, and Feedback Mechanisms (AC)3”.

595 We would like to acknowledge the constructive discussions with Susanne Crewell, that helped shaping the analysis. We would like to further acknowledge the helpful discussions with Vincenzo Levizzani and Tiina Nygård, and the assistance David Strack provided when working with IASI data.



References

- Aires, F.: Measure and Exploitation of Multisensor and Multiwavelength Synergy for Remote Sensing: 1. Theoretical Considerations, *Journal of Geophysical Research*, 116, D02 301, <https://doi.org/10.1029/2010JD014701>, 2011.
- August, T., Klaes, D., Schlüssel, P., Hultberg, T., Crapeau, M., Arriaga, A., O'Carroll, A., Coppens, D., Munro, R., and Calbet, X.: IASI on Metop-A: Operational Level 2 Retrievals after Five Years in Orbit, *Journal of Quantitative Spectroscopy and Radiative Transfer*, 113, 1340–1371, <https://doi.org/10.1016/j.jqsrt.2012.02.028>, 2012.
- Aumann, H., Chahine, M., Gautier, C., Goldberg, M., Kalnay, E., McMillin, L., Revercomb, H., Rosenkranz, P., Smith, W., Staelin, D., Strow, L., and Susskind, J.: AIRS/AMSU/HSB on the Aqua Mission: Design, Science Objectives, Data Products, and Processing Systems, *IEEE Transactions on Geoscience and Remote Sensing*, 41, 253–264, <https://doi.org/10.1109/TGRS.2002.808356>, 2003.
- Berrisford, P., Dee, D., Poli, P., Brugge, R., Fielding, M., Fuentes, M., Kållberg, P., Kobayashi, S., Uppala, S., and Simmons, A.: The ERA-Interim archive Version 2.0, <https://www.ecmwf.int/node/8174>, 2011.
- Blumstein, D., Chalon, G., Carlier, T., Buil, C., Hebert, P., Maciaszek, T., Ponce, G., Phulpin, T., Tournier, B., Simeoni, D., Astruc, P., Clauss, A., Kayal, G., and Jegou, R.: IASI Instrument: Technical Overview and Measured Performances, in: *Infrared Spaceborne Remote Sensing XII*, vol. 5543, pp. 196–207, International Society for Optics and Photonics, <https://doi.org/10.1117/12.560907>, 2004.
- Brunke, M. A., Stegall, S. T., and Zeng, X.: A Climatology of Tropospheric Humidity Inversions in Five Reanalyses, *Atmospheric Research*, 153, 165–187, <https://doi.org/10.1016/j.atmosres.2014.08.005>, 2015.
- Chang, L., Wen, S., Gao, G., Han, Z., Feng, G., and Zhang, Y.: Assessment of Temperature and Specific Humidity Inversions and Their Relationships in Three Global Reanalysis Products over the Arctic Ocean, *Journal of Applied Meteorology and Climatology*, 60, 493–511, <https://doi.org/10.1175/JAMC-D-20-0079.1>, 2021.
- Copernicus Climate Change Service (C3S): ERA5: Fifth generation of ECMWF atmospheric reanalyses of the global climate, <https://cds.climate.copernicus.eu/cdsapp#!/home>, <https://cds.climate.copernicus.eu/cdsapp#!/home>, accessed 18-02-2020, 2017.
- Devasthale, A., Sedlar, J., and Tjernström, M.: Characteristics of Water-Vapour Inversions Observed over the Arctic by Atmospheric Infrared Sounder (AIRS) and Radiosondes, *Atmospheric Chemistry and Physics*, 11, 9813–9823, <https://doi.org/10.5194/acp-11-9813-2011>, 2011.
- Dirksen, R. J., Sommer, M., Immler, F. J., Hurst, D. F., Kivi, R., and Vömel, H.: Reference Quality Upper-Air Measurements: GRUAN Data Processing for the Vaisala RS92 Radiosonde, *Atmospheric Measurement Techniques*, 7, 4463–4490, <https://doi.org/10.5194/amt-7-4463-2014>, 2014.
- Divakarla, M. G., Barnet, C. D., Goldberg, M. D., McMillin, L. M., Maddy, E., Wolf, W., Zhou, L., and Liu, X.: Validation of Atmospheric Infrared Sounder Temperature and Water Vapor Retrievals with Matched Radiosonde Measurements and Forecasts, *Journal of Geophysical Research*, 111, D09S15, <https://doi.org/10.1029/2005JD006116>, 2006.
- Durre, I. and Yin, X.: Enhanced radiosonde data for studies of vertical structure, *Bulletin of the American Meteorological Society*, 89, 1257–1262, <https://doi.org/10.1175/2008BAMS2603.1>, 2008.
- Durre, I., Vose, R. S., and Wuertz, D. B.: Overview of the Integrated Global Radiosonde Archive, *Journal of Climate*, 19, 53–68, <https://doi.org/10.1175/JCLI3594.1>, 2006.
- Ebell, K., Orlandi, E., Hünerbein, A., Löhnert, U., and Crewell, S.: Combining Ground-Based with Satellite-Based Measurements in the Atmospheric State Retrieval: Assessment of the Information Content, *Journal of Geophysical Research: Atmospheres*, 118, 6940–6956, <https://doi.org/10.1002/jgrd.50548>, 2013.



- ECMWF: ERA5: Data Documentation, <https://confluence.ecmwf.int/display/CKB/ERA5%3A+data+documentation>, last accessed 05-08-
635 2020, 2017.
- EUMETSAT: IASI Level 2: Product Guide, Tech. Rep. EUM/OPS-EPS/MAN/04/0033, EUMETSAT, Eumetsat-Allee 1, D-64295 Darmstadt, Germany, 2017.
- EUMETSAT: IASI L2 PPF v6.4 Validation Report, Tech. Rep. EUM/RSP/REP/18/974859, EUMETSAT, Eumetsat-Allee 1, D-64295 Darmstadt, Germany, 2018.
- 640 Gettelman, A., Walden, V. P., Miloshevich, L. M., Roth, W. L., and Halter, B.: Relative Humidity over Antarctica from Radiosondes, Satellites, and a General Circulation Model, *Journal of Geophysical Research*, 111, D09S13, <https://doi.org/10.1029/2005JD006636>, 2006.
- Graham, R. M., Hudson, S. R., and Maturilli, M.: Improved Performance of ERA5 in Arctic Gateway Relative to Four Global Atmospheric Reanalyses, *Geophysical Research Letters*, 46, 6138–6147, <https://doi.org/10.1029/2019GL082781>, 2019.
- Hersbach, H., Bell, B., Berrisford, P., Horányi, A., Sabater, J. M., Nicolas, J., Radu, R., Schepers, D., Simmons, A., Soci, C., et al.: Global
645 Reanalysis: Goodbye ERA-Interim, Hello ERA5, *ECMWF Newsletter*, 159, 17–24, 2019.
- Hersbach, H., Bell, B., Berrisford, P., Hirahara, S., Horányi, A., Muñoz-Sabater, J., Nicolas, J., Peubey, C., Radu, R., Schepers, D., Simmons, A., Soci, C., Abdalla, S., Abellan, X., Balsamo, G., Bechtold, P., Biavati, G., Bidlot, J., Bonavita, M., Chiara, G., Dahlgren, P., Dee, D., Diamantakis, M., Dragani, R., Flemming, J., Forbes, R., Fuentes, M., Geer, A., Haimberger, L., Healy, S., Hogan, R. J., Hólm, E., Janisková, M., Keeley, S., Laloyaux, P., Lopez, P., Lupu, C., Radnoti, G., Rosnay, P., Rozum, I., Vamborg, F., Villaume, S., and Thépaut,
650 J.-N.: The ERA5 Global Reanalysis, *Quarterly Journal of the Royal Meteorological Society*, 146, <https://doi.org/10.1002/qj.3803>, 2020.
- Hultberg, T. and August, T.: The Piecewise Linear Regression retrieval of temperature, humidity and ozone within the EUMETSAT IASI L2 PPF Version 6, Tech. rep., EUMETSAT, Eumetsat-Allee 1, D-64295 Darmstadt, Germany, 2014.
- Jeffries, M. O., Overland, J. E., and Perovich, D. K.: The Arctic Shifts to a New Normal, *Physics Today*, 66, 35–40, <https://doi.org/10.1063/PT.3.2147>, 2013.
- 655 Kwon, E.-H., Sohn, B. J., Smith, W. L., and Li, J.: Validating IASI Temperature and Moisture Sounding Retrievals over East Asia Using Radiosonde Observations, *Journal of Atmospheric and Oceanic Technology*, 29, 1250–1262, <https://doi.org/10.1175/JTECH-D-11-00078.1>, 2012.
- Langen, P. L., Graversen, R. G., and Mauritsen, T.: Separation of Contributions from Radiative Feedbacks to Polar Amplification on an Aquaplanet, *Journal of Climate*, 25, 3010–3024, <https://doi.org/10.1175/JCLI-D-11-00246.1>, 2012.
- 660 Löhnert, U., Turner, D. D., and Crewell, S.: Ground-Based Temperature and Humidity Profiling Using Spectral Infrared and Microwave Observations. Part I: Simulated Retrieval Performance in Clear-Sky Conditions, *Journal of Applied Meteorology and Climatology*, 48, 1017–1032, <https://doi.org/10.1175/2008JAMC2060.1>, 2009.
- Maturilli, M.: High resolution radiosonde measurements from station Ny-Ålesund (2017-04 et seq), <https://doi.org/10.1594/PANGAEA.914973>, 2020.
- 665 Maturilli, M. and Kayser, M.: Arctic warming, moisture increase and circulation changes observed in the Ny-Ålesund homogenized radiosonde record, *Theoretical and Applied Climatology*, 130, 1–17, <https://doi.org/10.1007/s00704-016-1864-0>, 2017.
- Menzel, W. P., Schmit, T. J., Zhang, P., and Li, J.: Satellite-Based Atmospheric Infrared Sounder Development and Applications, *Bulletin of the American Meteorological Society*, 99, 583–603, <https://doi.org/10.1175/BAMS-D-16-0293.1>, 2018.
- Mo, T.: Prelaunch Calibration of the Advanced Microwave Sounding Unit-A For NOAA-K, *IEEE Transactions on Microwave Theory and
670 Techniques*, 44, 10, <https://doi.org/10.1109/22.536029>, 1996.



- Morrison, H., de Boer, G., Feingold, G., Harrington, J., Shupe, M. D., and Sulia, K.: Resilience of Persistent Arctic Mixed-Phase Clouds, *Nature Geoscience*, 5, 11–17, <https://doi.org/10.1038/ngeo1332>, 2012.
- Murphy, D. M. and Koop, T.: Review of the Vapour Pressures of Ice and Supercooled Water for Atmospheric Applications, *Quarterly Journal of the Royal Meteorological Society*, 131, 1539–1565, <https://doi.org/10.1256/qj.04.94>, 2005.
- 675 Naakka, T., Nygård, T., and Vihma, T.: Arctic Humidity Inversions: Climatology and Processes, *Journal of Climate*, 31, 3765–3787, <https://doi.org/10.1175/JCLI-D-17-0497.1>, 2018.
- NOAA: NOAA KLM User’s Guide (February 2009 Revision), Tech. rep., U.S. Department of Commerce National Oceanic and Atmospheric Administration National Environmental Satellite, Data, and Information Service, 151 Patton Avenue, Asheville, North Carolina, USA, 2009.
- 680 Nygård, T., Valkonen, T., and Vihma, T.: Antarctic Low-Tropospheric Humidity Inversions: 10-Yr Climatology, *Journal of Climate*, 26, 5205–5219, <https://doi.org/10.1175/JCLI-D-12-00446.1>, 2013.
- Nygård, T., Valkonen, T., and Vihma, T.: Characteristics of Arctic Low-Tropospheric Humidity Inversions Based on Radio Soundings, *Atmospheric Chemistry and Physics*, 14, 1959–1971, <https://doi.org/10.5194/acp-14-1959-2014>, 2014.
- Olsen, E., Blaisdell, J., Iredell, L., and Susskind, J.: AIRS/AMSU/HSB Version 6 Retrieval Flow, Tech. rep., Jet Propulsion Laboratory, Pasadena, CA, 2017a.
- 685 Olsen, E., Fetzer, E. J., and et al.: AIRS/AMSU/HSB Version 6 Level 2 Product User Guide, Tech. rep., Jet Propulsion Laboratory, Pasadena, CA, 2017b.
- Parkinson, C.: Aqua: An Earth-Observing Satellite Mission to Examine Water and Other Climate Variables, *IEEE Transactions on Geoscience and Remote Sensing*, 41, 173–183, <https://doi.org/10.1109/TGRS.2002.808319>, 2003.
- 690 Rodgers, C. D.: *Inverse Methods for Atmospheric Sounding: Theory and Practice*, World Scientific, <https://doi.org/10.1142/3171>, 2000.
- Seidel, D. J., Berger, F. H., Diamond, H. J., Dykema, J., Goodrich, D., Immler, F., Murray, W., Peterson, T., Sisterson, D., Sommer, M., Thorne, P., Vomel, H., and Wang, J.: Reference Upper-Air Observations for Climate: Rationale, Progress, and Plans, *Bulletin of the American Meteorological Society*, 90, 361–369, <https://doi.org/10.1175/2008BAMS2540.1>, 2009.
- Serreze, M. C. and Barry, R. G.: Processes and Impacts of Arctic Amplification: A Research Synthesis, *Global and Planetary Change*, 77, 85–96, <https://doi.org/10.1016/j.gloplacha.2011.03.004>, 2011.
- 695 Serreze, M. C. and Barry, R. G.: *The Arctic Climate System*, Cambridge University Press, <https://doi.org/10.1017/CBO9781139583817>, 2014.
- Stroeve, J. C., Serreze, M. C., Holland, M. M., Kay, J. E., Malanik, J., and Barrett, A. P.: The Arctic’s Rapidly Shrinking Sea Ice Cover: A Research Synthesis, *Climatic Change*, 110, 1005–1027, <https://doi.org/10.1007/s10584-011-0101-1>, 2012.
- 700 Susskind, J., Barnet, C., and Blaisdell, J.: Retrieval of Atmospheric and Surface Parameters from AIRS/AMSU/HSB Data in the Presence of Clouds, *IEEE Transactions on Geoscience and Remote Sensing*, 41, 390–409, <https://doi.org/10.1109/TGRS.2002.808236>, 2003.
- Susskind, J., Schmidt, G. A., Lee, J. N., and Iredell, L.: Recent Global Warming as Confirmed by AIRS, *Environmental Research Letters*, 14, 044 030, <https://doi.org/10.1088/1748-9326/aafd4e>, 2019.
- Vihma, T., Screen, J., Tjernström, M., Newton, B., Zhang, X., Popova, V., Deser, C., Holland, M., and Prowse, T.: The Atmospheric Role in the Arctic Water Cycle: A Review on Processes, Past and Future Changes, and Their Impacts: Atmospheric Role in Arctic Water Cycle, *Journal of Geophysical Research: Biogeosciences*, 121, 586–620, <https://doi.org/10.1002/2015JG003132>, 2016.
- 705